JOURNAL OF GUIDANCE, CONTROL, AND DYNAMICS
Vol. 17, No. 1, January–February 1994

Effect of Pressure Stiffness on the Dynamics of Solid Rocket Motors

Eric R. Christensen*
Sverdrup Technology, Inc., Huntsville, Alabama 35806

This paper examines the effects of pressure on the dynamics of prestiffened structures such as the Space Shuttle solid rocket booster and the advanced solid rocket motor. Differences of up to 45% between analytical and test results for the SRB pitch/roll mode frequency are shown to be a result of an extra stiffness term resulting from the applied pressure load. In the past, these effects have been modeled empirically based on test data. In this paper, these pressure stiffness terms are derived analytically for various types of line and area finite elements. These new elements have been implemented as dummy elements in COSMIC NASTRAN and can be easily added to any existing NASTRAN finite element model. The pressure stiffness elements are tested on some simple example problems and are used in existing SRB NASTRAN models to analytically match the quarter-scale SRB pitch/roll test frequencies with differences of less than 5%.

Introduction

THE advanced solid rocket motor (ASRM) (Fig. 1) is being developed as a replacement for the solid rocket booster (SRB) presently being used in the Space Shuttle system. The ASRM offers several advantages over the SRB. An increase in the diameter of the motor from 146 to 150 in. and an improvement in the propellant and grain design will result in greater payload capability. Reliability has been improved by replacing pinned joints with bolted and welded joints, an improved nozzle, integral aft segment stiffeners, and an improved igniter. As part of the analysis effort of verifying the ASRM design, a large three-dimensional NASTRAN finite element model (FEM) of the ASRM structure is being constructed for use in determining the dynamic characteristics of the structure and its response to various loadings.

In the past, the mathematical models of the SRB have not included an important dynamic effect. As the solid propellant in the booster burns, high pressure gases of up to about 1000 psi are present. This pressure stiffens the structure and significantly increases the natural frequencies of certain modes. This extra stiffness is a nonlinear effect and is accounted for through the initial stress stiffness matrix that can be calculated by the differential stiffness routines in NASTRAN or other finite element codes. In the formulation of this initial stress stiffness matrix it is assumed that the loading is constant in both magnitude and direction. The direction of the pressure loading, however, will violate this assumption since it always remains normal to the surface over which it is applied and will change direction as the structure deforms. The calculated natural frequencies will be in error unless this change in direction is accounted for. The pressure thus has two effects on the natural frequencies. The first effect is due to stress stiffening and can be calculated by NASTRAN. The second effect is due to the change in direction of the applied pressure and cannot be calculated by NASTRAN. This second effect is called the pressure stiffness effect and is more pronounced in some modes than in others. In the case of the SRB it is most pronounced in the "pitch/roll" mode which is the fundamental system mode. In the past, modal analyses of the SRB have not been able to take the pressure stiffness effect into account analytically but have relied instead on test data to determine it. Differences of up to 45% between calculated frequencies and test frequencies for the pitch/roll modes have been found. These differences are illustrated in Fig. 2 which shows a comparison between test and analytical results for the quarter-scale SRB (QSSRB) test fixture. Once determined by test data, the pressure stiffness effect was empirically included in the SRB FEMs.

The objective of this work has been to formulate a method by which the pressure stiffness effect can be analytically determined and included in the NASTRAN FEM of the ASRM. A key objective has been to test the formulation on the QSSRB FEM and analytically match the test results shown in Fig. 2.

The effects of so-called follower forces, i.e., forces which "follow" the deformations of the structure, have been investigated to some extent in the past. Hibbitt[1] demonstrated the significance of follower forces in the finite element analyses of various types of problems. He showed that effects due to the follower forces can be represented by extra stiffness terms called the load stiffness or pressure stiffness terms, but he presents no numerical examples.

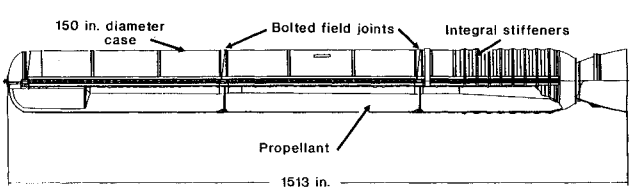

Fig. 1 Advanced solid rocket motor design.

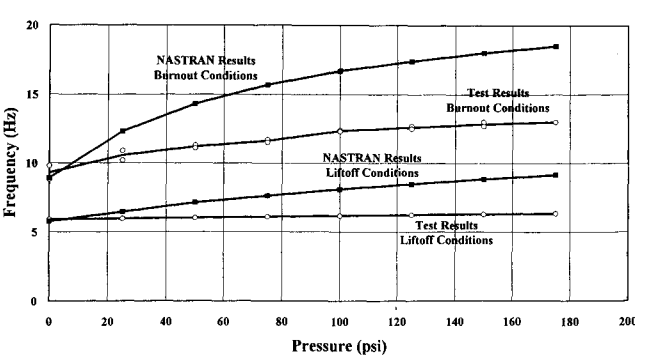

Fig. 2 QSSRB roll mode frequency.

Presented as Paper 91-0940 at the AIAA/ASME/ASCE/AHS/ASC 32nd Structures, Structural Dynamics, and Materials Conference, Baltimore, MD, April 8–10, 1991; received March 6, 1992; revision received April 20, 1993; accepted for publication April 22, 1993.

*Supervisor, Structural Dynamics Section, 620 Discovery Drive. Associate Fellow AIAA.

The pressure stiffness is also important in certain types of buckling problems. A classical example is the buckling of a thin, elastic, circular ring under external pressure, which was studied by Boresi.[2] Other investigators[3-5] extended the analysis in Ref. 2 to the buckling of more general shells. A nonlinear finite element analysis of elastic structures subject to more general nonconservative loading was investigated in Refs. 6 and 7, which focus on the stability behavior of such systems and use the natural mode technique to derive expressions for the load correction or pressure stiffness matrix. Application of the theory is limited to beam elements. Numerical examples, including divergence and flutter types of instability, are presented. Herting and Haggenmacher[8] developed a triangular MSC/NASTRAN finite element to represent the stiffness of pressure loads on surfaces that remain flat as they deform. They presented a few simple examples that show this effect on buckling and normal mode analyses.

The objective of the current work is to formulate a method by which the pressure stiffness effect can easily be included in the NASTRAN model of the ASRM. In the next section the pressure stiffness terms are derived for a line element, and it is shown that the bending terms are negligible. Based on those results, the pressure stiffness for a triangular surface element is derived in a way similar to that of Ref. 8. The derivation is then extended to a quadrilateral surface element, implemented in COSMIC NASTRAN, and applied to the FEMs of the SRB and ASRM.

General Formulation of the Pressure Stiffness

The existence of the pressure stiffness terms for a general element can be demonstrated by examining a pressure force $\{p(\{u\})\}$ where $\{u\}$ represents the displacements of the structure. In all subsequent equations vector quantities are represented by braces and matrices are indicated by brackets. A small change in the displacements $d\{u\}$ will cause a change of $d\{p\}$ in the pressure force as follows:

$$d\{p\} = \frac{\partial\{p\}}{\partial\{u\}}\, d\{u\} = [K_p]\, d\{u\} \tag{1}$$

where $[K_p] = \partial\{p\}/\partial\{u\}$ is the pressure stiffness matrix.

To calculate $[K_p]$ it is necessary to have expressions for the virtual work done by the pressure force during the deformations of a general structure. Consider a structure as it deforms from its initial state to its deformed state. For equilibrium to be satisfied the virtual work done by the internal forces must equal the virtual work done by the external forces. The external forces can be divided into body forces (including inertial forces) and applied surface forces. The applied surface forces can be subdivided into applied pressure forces and all other applied surface forces. In general, the deformations can be large and the loading deformation dependent. Using the total Lagrangian approach, the equilibrium expression for the deformable body can be written as

$$\int_{V_0} \delta\{E\}^T\{S\}\, dV_0 - \int_{V_0} \rho_0 \delta\{u\}^T\{f_B\}\, dV_0 - \int_{S_\sigma} \delta\{u\}^T\{T\}\, dS - \int_{S_\sigma} p\,\delta\{u\}^T\{n\}\, dS = 0 \tag{2}$$

where δ represents the variational operator, $\{E\}$ is the vector of Green strains, $\{S\}$ is the vector of second Piola-Kirchoff stresses, V_0 is the initial undeformed volume of the structure, ρ_0 is the mass density in the undeformed structure, $\{f_B\}$ is the vector of applied body forces, p is the magnitude of the pressure, $\{n\}$ is a unit normal to the surface S_σ in the direction of the pressure, and $\{T\}$ is the vector of applied surface forces other than pressure. In Eq. (2) the first integral represents the virtual work done by the internal forces, the second integral represents the virtual work done by the applied body forces, the last integral represents the virtual work done by the applied pressure forces, and the third integral is the virtual work done by any other applied surface forces. Since the pressure is a follower force, $\{n\}$ is a function of the displacements $\{u\}$ and the virtual work done by the pressure force is deformation dependent.

Equation (2) is the equilibrium expression for a large displacement problem and is, in general, a nonlinear expression that must be solved incrementally. One way to do this is by making a finite element approximation for the incremental displacements. The details of how to do this for the first three integrals in Eq. (2) can be found in many places (e.g., Ref. 9). When this is done, the first three integrals in Eq. (2) will result in the following:

$$\int_{V_0} \delta\{E\}^T\{S\}\, dS_\sigma - \int_{V_0} \rho_0 \delta\{u\}^T\{f_B\}\, dV_0 - \int_{S_\sigma} \delta\{u\}^T\{T\}\, dS = \delta\{q\}^T\Big\{[M]\{\ddot{q}\} + \big([K_L]+[K_U]+[K_S]\big)\Delta\{q\} + \Delta\{F\}\Big\} \tag{3}$$

where $\delta\{q\}$ is the virtual displacement vector, $\Delta\{q\}$ the incremental nodal displacement vector, $[K_L]$ the linear (small displacement) stiffness matrix, $[K_U]$ the large displacement stiffness matrix, $[K_S]$ the initial stress or differential stiffness matrix, $[M]$ the mass matrix, and $\Delta\{F\}$ the incremental force vector including the applied and residual force equilibrium terms. The incremental displacement $\Delta\{q\}$ represents the change in the displacements from the equilibrium position found in the preceding iteration. The large displacement stiffness matrix $[K_U]$ is a function of the total displacements $\{q\}$ and is usually calculated using the displacements found in the preceding iteration. Both the initial stress stiffness matrix and the incremental force vector are functions of the stresses and can be determined at each time step by using the values for $\{S\}$ determined from the preceding iteration. Substitution of the finite element approximation into the fourth integral in Eq. (2) will result in

$$-\int_{S_\sigma} p\,\delta\{u\}^T\{n\}\, dS = \delta\{q\}^T\big([K_p]\Delta\{q\} - \{F_p\}\big) \tag{4}$$

where $\{F_p\}$ represents the nodal force vector due to the pressure and $[K_p]$ is the pressure stiffness matrix, which in general is deformation dependent. If Eqs. (3) and (4) are substituted into Eq. (2), the following incremental differential equation of motion is obtained:

$$[M]\{\ddot{q}\} + \big([K_L]+[K_U]+[K_S]+[K_p]\big)\Delta\{q\} = \Delta\{F\} \tag{5}$$

To solve Eq. (5) exactly as a function of time would require a full nonlinear, incremental dynamic transient analysis. If, on the other hand, it is only desired to determine the natural frequencies of small vibrations about some static equilibrium position, then the following procedure can be followed. First, iteratively determine the static equilibrium position $\{q_0\}$ and the corresponding state of stress $\{S_0\}$. In Eq. (5) $[K_U]$ and $[K_p]$ are functions of $\{q_0\}$, and $[K_S]$ is a function of $\{S_0\}$, so that for a given equilibrium position $\{q_0\}$, all of the matrices on the left-hand side of Eq. (5) will be constant, and it can be solved as an eigenvalue problem with the right-hand side equal to zero.

The COSMIC NASTRAN rigid format solution 13 entitled "Normal Modes with Differential Stiffness" is an approximate solution of Eq. (5), which does not include all of the stiffness terms. The $[K_U]$ and $[K_p]$ terms are not included, and only a single interation is used in the solution for $\{q_0\}$. Neglecting the $[K_U]$ terms should not cause significant errors as long as the strains remain small. Neglecting the $[K_p]$ terms, however, can cause large errors. In the modified solution 13 developed in this paper, the $[K_p]$ terms will be added into the

differential stiffness matrix. The other approximations inherent in the existing solution 13 are not addressed in this paper.

Planar Line Elements

To illustrate the effect of the pressure stiffness, a simple example problem consisting of a 10×10-in. square free-free frame with the properties shown in Fig. 3 is presented. The frame is loaded by an internal pressure p of 100 lb/in. The frame is modeled by four massless two-node plane beam elements (CBARs in NASTRAN) with the mass represented by four concentrated masses (CONM1s) at each corner. Each CONM1 has a mass of 1.0 lb-s^2/in. and an inertia of 1.0 in.-lb-s^2. The model has a total of 12 unconstrained degrees of freedom, two translations, and one rotation at each of the four nodes. The natural frequencies of the unloaded frame as calculated by COSMIC NASTRAN are listed in the second column of Table 1. Notice that there are three zero frequency rigid body modes representing two rigid body translations and one rigid body rotation. The application of the pressure loading stretches the structure, increasing its stiffness and changing the natural frequencies. Using the unmodified COSMIC NASTRAN solution 13 results in the set of natural frequencies listed in column three of Table 1. Notice that there are no longer three zero frequencies but that the mode-3 frequency has become 1.5759 Hz. Examination of mode shape 3, however, indicates that mode 3 represents a rigid body rotation. A physical explanation of the phenomenon is illustrated in Fig. 4, which shows that by neglecting the change in direction of the pressure force a fictitious moment is introduced that tends to move the structure back toward its equilibrium position. This fictitious moment is proportional to the angular motion of the frame and is equivalent to a fictitious grounded rotational spring. The fictitious spring artificially adds stiffness to the system and results in a nonzero frequency. The larger the pressure is, the greater this effect will be.

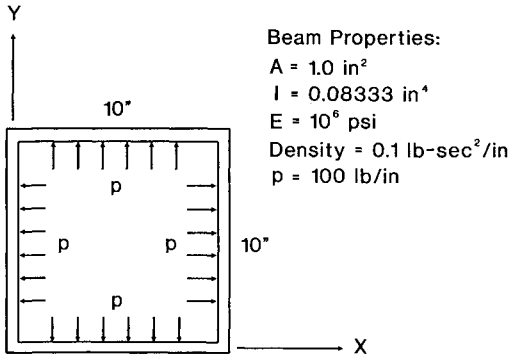

Fig. 3 Pressurized square frame.

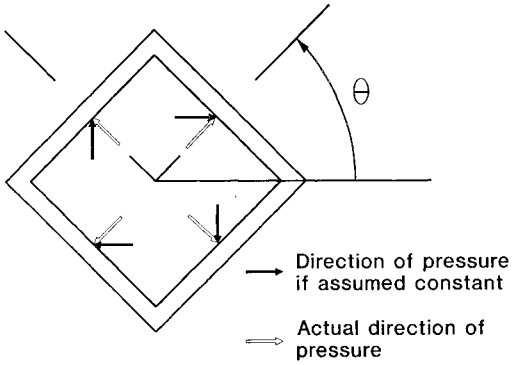

Fig. 4 Forces on rotated frame.

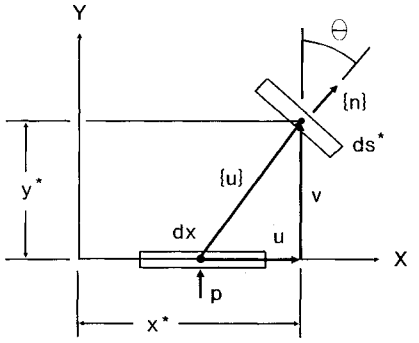

Fig. 5 Beam element kinematics.

Table 1 Natural frequencies of a pressurized square frame

	Natural frequency, Hz		
Mode no.	No preload	Preload without pressure stiffness	Preload with pressure stiffness
1	4.4E-07	4.1E-07	2.6E-07
2	2.2E-07	2.4E-07	5.7E-07
3	2.5E-07	1.5759	2.4E-04
4	7.1176	7.3280	7.4989
5	29.0576	29.7752	29.7750
6	40.8665	41.2711	41.2634
7	40.8665	41.2711	41.2634
8	50.8300	51.0840	51.0835
9	71.1763	71.1763	71.1585
10	71.1763	71.1763	71.1941

To correct the error in the preceding example, it is necessary to add the pressure stiffness matrix $[K_p]$ to the overall stiffness matrix and take into account the virtual work done by the pressure force as it rotates. One way to do this is by reference to Fig. 5 in which a small length dx of the beam is shown in its undeformed and deformed positions. The beam is assumed to remain within the plane of the paper at all times. The undeformed position of the element is $(x, 0)$ and it deforms an amount $\{u\}$ to (x^*, y^*) with a deformed length of ds^*. The values of x^* and y^* can be found from

$$x^* = x + u, \qquad y^* = v \tag{6}$$

where $\{u\} = u\{i\} + v\{j\}$ and $\{i\}$ and $\{j\}$ are unit vectors in the x and y directions. If $\{n\}$ is a unit normal to the beam element, the virtual work done by the pressure force can be found from Eq. (2)

$$\delta W_p = \int_L p\{n\} \cdot \delta\{u\}\, ds \tag{7}$$

where $\delta\{u\} = \delta u\{i\} + \delta v\{j\}$ is the virtual displacement and L the deformed length of the beam element. From the geometry shown in Fig. 5 it can be seen that

$$\begin{aligned} \{n\}\, ds^* &= \sin\theta\, ds^*\{i\} + \cos\theta\, ds^*\{j\} \\ &= -dy^*\{i\} + dx^*\{j\} \end{aligned} \tag{8}$$

where dx^* and dy^* represent the projection of ds^* on the x and y axes. Expressions for dx^* and dy^* can be found by differentiating Eq. (6)

$$dx^* = \left(1 + \frac{du}{dx}\right) dx, \qquad dy^* = \frac{dv}{dx}\, dx \tag{9}$$

If Eqs. (8) and (9) and the expression for virtual displacement are substituted into Eq. (7), the following expression for the virtual work is obtained:

$$\delta W_p = p \int_0^{\ell} \left[-\delta u \frac{dv}{dx} + \delta v \left(1 + \frac{du}{dx}\right) \right] dx \tag{10}$$

In Eq. (10) ℓ is the undeformed element length and the pressure has been moved out of the integral since it is assumed constant. For a two-dimensional, two-noded beam, the finite element approximations for the displacements u and v can be expressed as follows:

$$u = [N_u(x)]\{q\}, \quad v = [N_v(x)]\{q\} \tag{11}$$

where $\{q\}^T = \lfloor u_1 \quad v_1 \quad \theta_1 \quad u_2 \quad v_2 \quad \theta_2 \rfloor$ with $[N_u]$ and $[N_v]$ being element shape function matrices and u_i, v_i, and θ_i being the x displacement, y displacement, and rotation, respectively, at node $i = 1, 2$. Substituting Eq. (11) into Eq. (10) results in

$$\delta W_p = \delta\{q\}^T(-[K_p]\{q\} + \{F_p\}) \tag{12}$$

$$[K_p] = p\int_0^\ell \left([N_u]^T \frac{d[N_v]}{dx} - [N_v]^T \frac{d[N_u]}{dx}\right) dx \tag{13}$$

$$\{F_p\} = p\int_0^\ell [N_v]^T \, dx \tag{14}$$

Note that $\{F_p\}$ is the usual applied force term due to pressure. The sign of the pressure stiffness matrix $[K_p]$ has been defined as negative so that it can be added to the other terms in the global stiffness matrix rather than subtracted. Also notice that Eq. (13) for $[K_p]$ in general will result in a nonsymmetric matrix. However, in the case of a constant pressure acting over an enclosed volume it has been shown[10] that the pressure is a conservative load, and thus the nonsymmetric parts of the pressure stiffness matrix will cancel out when they are assembled into the global stiffness matrix. All of the example problems studied in this paper will assume constant pressures applied over enclosed volumes so that the nonsymmetric parts of the $[K_p]$ matrices will always cancel out.

If the usual expressions for $[N_u]$ and $[N_v]$ are substituted into Eq. (13) and the integrals are evaluated, the pressure stiffness matrix can be expressed as follows:

$$[K_p] = \begin{bmatrix} 0 & -\frac{p}{2} & -\frac{p\ell}{12} & 0 & \frac{p}{2} & \frac{p\ell}{12} \\ \frac{p}{2} & 0 & 0 & -\frac{p}{2} & 0 & 0 \\ -\frac{p\ell}{12} & 0 & 0 & \frac{p\ell}{12} & 0 & 0 \\ 0 & -\frac{p}{2} & \frac{p\ell}{12} & 0 & \frac{p}{2} & -\frac{p\ell}{12} \\ \frac{p}{2} & 0 & 0 & -\frac{p}{2} & 0 & 0 \\ \frac{p\ell}{12} & 0 & 0 & -\frac{p\ell}{12} & 0 & 0 \end{bmatrix} \tag{15}$$

In Eq. (15), the rows and columns are defined consistent with the definition of $\{q\}$ in Eqs. (11) and (12). In most cases, the terms associated with the rotational degrees of freedom are very small and can be neglected, especially as the number of elements used increases. The reason for this is illustrated in Fig. 6. Notice that the difference between the change in rotation of the pressure force for each case shown will be small, especially as the element length ℓ decreases. If the rotational terms are neglected, the $p\ell/12$ terms in Eq. (15) can be replaced by zeros.

The pressure stiffness matrix for the square frame example was calculated using Eq. (15) with and without the rotational terms, and the natural frequencies were calculated using a FORTRAN program written by the author. The results are listed in column 4 of Table 1 where it can be seen that there are once again three zero frequencies. The results with and without the rotational terms agreed to within four decimal places. The effect of the pressure stiffness on the higher frequencies was less dramatic, although the first elastic frequency has increased by 2.3%. For the higher modes the change in direction of the pressure on one part of the structure is cancelled out by the change in direction on other portions of the structure so the pressure stiffness has a much smaller effect on these modes.

Triangular and Quadrilateral Surface Elements

Based on the results obtained from the line element examples as well as the reasoning behind Fig. 6, it is assumed that the contribution of the rotational degrees of freedom to the pressure stiffness of the surface elements is negligible. This greatly simplifies the derivation because it makes it unnecessary to include the bending terms and the problem becomes one of determining the pressure stiffness for a triangular surface that remains flat as it displaces.

Consider a triangular surface loaded by a constant pressure p as pictured in Fig. 7. The undeformed element has nodes at points A_0, B_0, and C_0 that deflect by the amounts $\{u_A\}$, $\{u_B\}$, and $\{u_C\}$ to points A, B, C. Let $\{n\}$ be a unit normal defining the direction of the applied pressure. If A_T is the total area of the triangle, then

$$2A_T\{n\} = \{r_{AB}\} \times \{r_{BC}\} = (\{r_B\} - \{r_A\}) \times (\{r_C\} - \{r_B\}) \tag{16}$$

where $\{r_A\}$, $\{r_B\}$, and $\{r_C\}$ are the position vectors of points A, B, and C. But

$$\begin{aligned} \{r_A\} &= \{r_{A_0}\} + \{u_A\} \\ \{r_B\} &= \{r_{B_0}\} + \{u_B\} \\ \{r_C\} &= \{r_{C_0}\} + \{u_C\} \end{aligned} \tag{17}$$

where $\{r_{A_0}\}$, $\{r_{B_0}\}$, and $\{r_{C_0}\}$ are the position vectors of points A_0, B_0, and C_0. Substituting Eqs. (17) into Eq. (16) and expanding results in the following:

$$\begin{aligned} 2A_T\{n\} = {} & [\tilde{r}_{A_0B_0}]\{r_{B_0C_0}\} + ([\tilde{r}_{B_0C_0}] + [\tilde{u}_C])\{u_A\} \\ & + ([\tilde{r}_{C_0A_0}] + [\tilde{u}_A])\{u_B\} + ([\tilde{r}_{A_0B_0}] + [\tilde{u}_B])\{u_C\} \end{aligned} \tag{18}$$

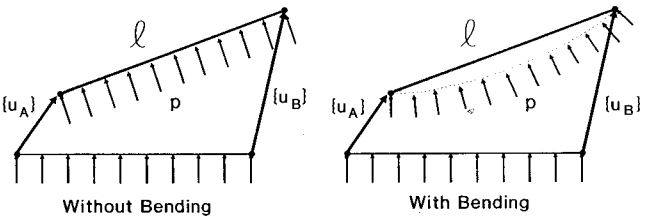

Fig. 6 Effect of neglecting bending terms.

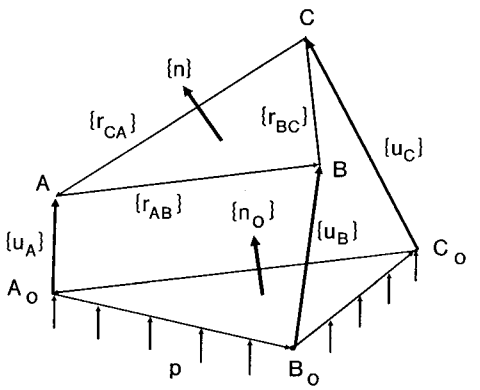

Fig. 7 Triangular surface element.

In Eq. (18), the cross products have been replaced by equivalent matrix products as follows. If $\{a\}$ and $\{b\}$ are two 3×1 vectors, then $\{a\} \times \{b\}$ can be written as $[\tilde{a}]\{b\}$ where

$$[\tilde{a}] = \begin{bmatrix} 0 & -a_3 & a_2 \\ a_3 & 0 & -a_1 \\ -a_2 & a_1 & 0 \end{bmatrix} \tag{19}$$

Note that $[\tilde{a}] = -[\tilde{a}]^T$. The virtual work done by the pressure p is

$$\delta W_p = \int_{A_T} p\delta\{u\}^T\{n\}\, dA \tag{20}$$

where $\{u\}$ is the displacement field within the element. Since all of the displaced points are assumed to lie in the plane formed by A, B, and C, $\{u\}$ can be expressed as follows:

$$\begin{aligned} \{u\} &= L_A\{u_A\} + L_B\{u_B\} + L_C\{u_C\} \\ \delta\{u\} &= L_A\delta\{u_A\} + L_B\delta\{u_B\} + L_C\delta\{u_C\} \end{aligned} \tag{21}$$

where L_A, L_B, and L_C are triangular area coordinates.[9] Substituting Eqs. (21) and (18) into Eq. (20) and integrating over the element area results in the following expression for the virtual work:

$$\delta W_p = \delta\{q\}^T\left(\frac{p}{6}\right)\left(\begin{bmatrix} [\tilde{r}_{A_0B_0}] \\ [\tilde{r}_{A_0B_0}] \\ [\tilde{r}_{A_0B_0}] \end{bmatrix}\{r_{B_0C_0}\} + \begin{bmatrix} [\tilde{r}_{B_0C_0}]+[\tilde{u}_C] & [\tilde{r}_{C_0A_0}]+[\tilde{u}_A] & [\tilde{r}_{A_0B_0}]+[\tilde{u}_B] \\ [\tilde{r}_{B_0C_0}]+[\tilde{u}_C] & [\tilde{r}_{C_0A_0}]+[\tilde{u}_A] & [\tilde{r}_{A_0B_0}]+[\tilde{u}_B] \\ [\tilde{r}_{B_0C_0}]+[\tilde{u}_C] & [\tilde{r}_{C_0A_0}]+[\tilde{u}_A] & [\tilde{r}_{A_0B_0}]+[\tilde{u}_B] \end{bmatrix}\{q\}\right) \tag{22}$$

where $\{q\}^T = [\{u_A\}\ \{u_B\}\ \{u_C\}]$ is the element nodal displacement vector. The first term in Eq. (22) results in the usual element force term due to the applied pressure. The second term is due to the pressure stiffness and yields the pressure stiffness matrix $[K_p]$. As can be seen from Eq. (22), $[K_p]$ is a function of the displacements. However, we will assume that the displacements are much smaller than the element dimensions so that they can be neglected in calculating $[K_p]$, which can then be written as follows:

$$[K_p] = -\frac{p}{6}\begin{bmatrix} [\tilde{r}_{B_0C_0}] & [\tilde{r}_{C_0A_0}] & [\tilde{r}_{A_0B_0}] \\ [\tilde{r}_{B_0C_0}] & [\tilde{r}_{C_0A_0}] & [\tilde{r}_{A_0B_0}] \\ [\tilde{r}_{B_0C_0}] & [\tilde{r}_{C_0A_0}] & [\tilde{r}_{A_0B_0}] \end{bmatrix} \tag{23}$$

As before, the sign of $[K_p]$ has been defined as negative so that it can be added to the other terms in the global stiffness matrix rather than subtracted. Equation (23) is essentially the same equation as Eq. (30) in Ref. 8.

The four-node quadrilateral element is formed by subdividing the quadrilateral into four overlapping subtriangles. The pressure stiffness matrix is formed by assembling the subtriangular element matrices into an overall stiffness matrix for the quadrilateral element.

The triangular and quadrilateral elements were implemented in COSMIC NASTRAN using the CDUM1 and CDUM2 dummy elements, respectively. The CDUM1 and CDUM2 elements are placed concurrently with any triangular or quadrilateral surface (such as a CTRIA2, CQUAD4, or a face of a CIHEX1, etc.) on which a pressure force is applied. Care must be taken that the order of element node numbers on the CDUM1 or CDUM2 element is consistent with the direction of the applied pressure. The elements were formulated so that the node numbering is the same as that required for the use of a PLOAD2 card. In addition, only the symmetric part of the pressure stiffness matrix in Eq. (23) was kept.

Solid Rocket Booster and Advanced Solid Rocket Motor Models

Quarter-Scale Solid Rocket Booster Analysis/Test Comparison

The CDUM1 and CDUM2 elements were applied to an existing NASTRAN model of the SRB to see if the test results shown in Fig. 2 could be predicted analytically. This model is pictured in Fig. 8 and consists of approximately 2500 nodes and 3250 elements. To this model were added 95 CDUM1 and 700 CDUM2 pressure stiffness elements. The flexibility of the test support fixture was included in the model.

The resulting pitch/roll mode frequencies for both the liftoff and the burnout configuration are plotted in Fig. 9. In the liftoff configuration, the propellant is modeled by CQUAD1 shear plates. Because of this, the internal pressure is applied to the case rather than directly to the propellant elements. A room temperature propellant shear modulus of $G' = 415$ psi was used. In the burnout configuration, the CQUAD1 propellant elements have been deleted from the model. The analyses were run for pressures ranging from 0 to 500 psi both with and without the CDUM elements. As can be seen from Fig. 9, excellent agreement was obtained between the analytical and test results with a difference of only 2.25% for the liftoff configuration and 4.6% for burnout at the maximum QSSRB test pressure of 175 psi.

Advanced Solid Rocket Motor Models

The CDUM1 and CDUM2 element were next applied to an existing NASTRAN model of the ASRM. This model is very

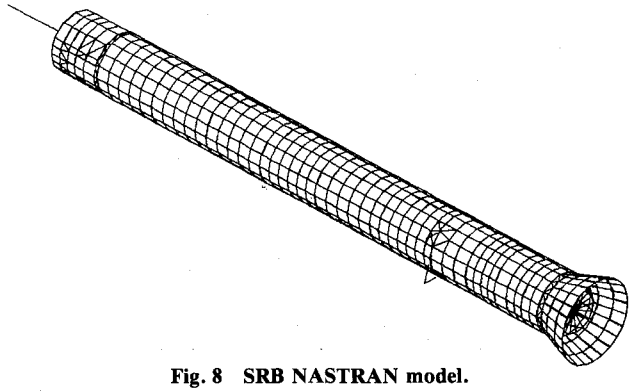

Fig. 8 SRB NASTRAN model.

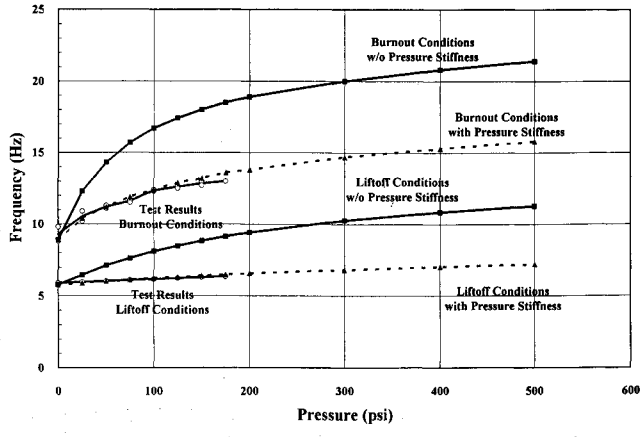

Fig. 9 QSSRB roll mode frequencies.

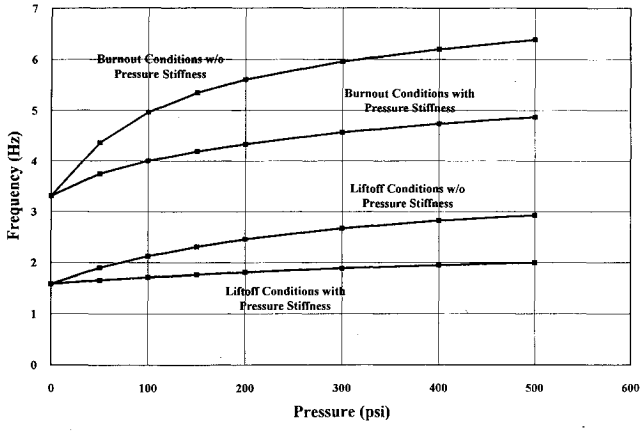

Fig. 10 ASRM mode-1 (roll mode) frequency.

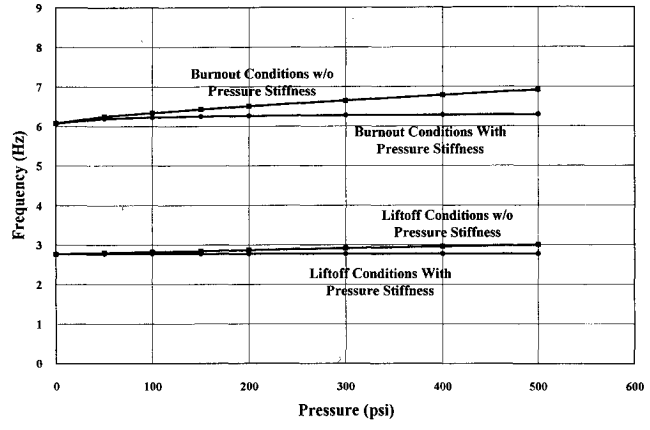

Fig. 11 ASRM mode-2 frequency.

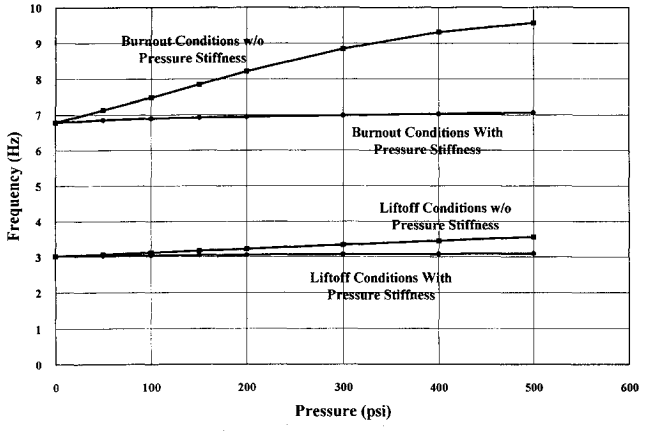

Fig. 12 ASRM mode-3 frequency.

similar to the model of the SRB and has basically the same number and types of elements. For this analysis, the external tank attach struts are assumed to be fixed because these are the boundary conditions used to determine the range of allowable frequencies of the booster. This frequency range is defined by the overall Shuttle control system, and if the booster frequencies are outside of this range the control system must be modified. For the control system to be stable, the first three modes in the liftoff configuration should fall within the following limits at 500 psi:

First mode: $1.70 \text{ Hz} \leq \omega_1$

Second mode: $2.69 \leq \omega_2 \leq 3.39$ Hz

Third mode: $3.01 \leq \omega_3 \leq 3.80$ Hz

The frequencies of the first three modes for both liftoff and burnout configurations are plotted in Figs. 10–12. Notice that all three modes will satisfy the conditions stated earlier. As was already shown, the effect of the pressure stiffness is dependent on the mode shape. As with the SRBs, the pressure stiffness has the greatest effect on the pitch/roll mode. For modes 2 and 3 the effect is less apparent, although there is a 36% error in the mode-3 frequency for the burnout condition if the pressure stiffness is not included in the analysis.

Conclusions

As has been demonstrated by previous experience with the solid rocket boosters and by the examples in this report, the pressure stiffness will have a significant effect on the dynamics of the advanced solid rocket motor (ASRM). Unless the pressure stiffness terms are added into the overall stiffness matrix or otherwise corrected for, the frequencies calculated for certain modes will contain large errors. The pressure stiffness tends to decrease the natural frequency for some modes and increase it for others, depending on the mode shape. For "rolling" type modes in which a large amount of rigid body motion is occurring (such as the ASRM pitch/roll mode), the effect is generally to decrease the natural frequency. In modes where there is more elastic deformation, the effect generally will be to increase the natural frequency, although this will be determined by the actual mode shape. The effect becomes greater as the pressure loading is increased. It is most pronounced for the lower modes and generally becomes insignificant for the higher modes. Also, for the types of problems of interest in this paper, the pressure stiffness associated with rotational degrees of freedom is negligible.

By matching the quarter-scale solid rocket booster test results with less than 5% difference, the pressure stiffness elements presented in this paper have demonstrated the ability to analytically predict pressure stiffness effects. The new elements are relatively simple to implement and can easily be added to existing NASTRAN models. They should be able to accurately predict the pressure stiffness effects in the ASRM models.

The pressure stiffness elements have been formulated assuming a constant pressure applied over an enclosed volume. For most of the computations involving the dynamics of the ASRM this is a good approximation. However, in reality there is a pressure gradient down the length of the ASRM case and a small opening through the nozzle. For this type of loading the nonsymmetric terms in the stiffness matrix will not completely cancel out, and a nonsymmetric global stiffness matrix results. The same basic element formulation holds, but the actual computational procedure changes due to the nonsymmetric nature of the matrices involved. Even though this is expected to be a small effect, a follow-on task has been undertaken that will allow this type of loading to be analyzed and will provide some bounds on the accuracy of the methodology presented in this paper.

Acknowledgment

I would like to thank Frank M. Bugg, of the Marshall Space Flight Center, who acted as the task initiator for this project and without whose invaluable assistance its successful completion would have been impossible.

References

[1]Hibbitt, H. D., "Some Follower Forces and Load Stiffness," *International Journal for Numerical Methods in Engineering,* Vol. 14, No. 6, 1979, pp. 937–941.

[2]Boresi, A. P., "A Refinement of the Theory of Buckling of Rings Under Uniform Pressure," *Journal of Applied Mechanics,* Vol. 22, No. 1, 1955, pp. 95–102.

[3]Boresi, A. P., and Langhaar, H. L., "Buckling and Post-Buckling Behavior of a Cylindrical Shell Subjected to External Pressure," Theoretical and Applied Mechanics Rept. 93, Univ. of Illinois, 1956.

[4]Almroth, B., and Brush, D., "Buckling of a Finite Length Cylindrical Shell Under a Circumferential Band of Pressure," *Journal of the Aeronautical Sciences,* Vol. 28, No. 7, 1961, pp. 573–578.

[5]Almroth, B., "Buckling of a Cylindrical Shell Subjected to Non-Uniform External Pressure," *Journal of Applied Mechanics,* Vol. 29, Dec. 1962, pp. 675–682.

[6]Argyris, J. H., and Symeonidis, S., "Nonlinear Finite Element Analysis of Elastic Systems Under Nonconservative Loading—Natural Formulation. Part I. Quasistatic Problems," *Computer Methods in Applied Mechanics and Engineering,* Vol. 26, 1981, pp. 75–123.

[7]Argyris, J. H., and Symeonidis, S., "Nonlinear Finite Element Analysis of Elastic Systems Under Nonconservative Loading—Natural Formulation. Part II. Dynamic Problems," *Computer Methods in Applied Mechanics and Engineering,* Vol. 28, 1981, pp. 241–258.

[8]Herting, D. N., and Haggenmacher, G. W., "Pressure Follower Matrix For Geometric Nonlinear Finite Element Analysis," MSC/NASTRAN User's Conference, March 1987.

[9]Zienkiewicz, O. C., *The Finite Element Method,* 3rd ed., McGraw-Hill, New York, 1977, pp. 500–526.

[10]Bodner, S. R., "On the Conservativness of Various Distributed Force Systems," *Journal of the Astronautical Sciences,* Vol. 25, No. 2, 1958, pp. 132, 133.